



HAL
open science

Analysis of Compressing PAPR-Reduced OFDM IQ Samples for Cloud Radio Access Network

A. Shehata, Philippe Mary, M. Crussiere

► **To cite this version:**

A. Shehata, Philippe Mary, M. Crussiere. Analysis of Compressing PAPR-Reduced OFDM IQ Samples for Cloud Radio Access Network. *IEEE Transactions on Broadcasting*, 2022, 68 (3), pp.765-779. 10.1109/TBC.2022.3176198 . hal-03719865

HAL Id: hal-03719865

<https://hal.science/hal-03719865>

Submitted on 21 Jul 2022

HAL is a multi-disciplinary open access archive for the deposit and dissemination of scientific research documents, whether they are published or not. The documents may come from teaching and research institutions in France or abroad, or from public or private research centers.

L'archive ouverte pluridisciplinaire **HAL**, est destinée au dépôt et à la diffusion de documents scientifiques de niveau recherche, publiés ou non, émanant des établissements d'enseignement et de recherche français ou étrangers, des laboratoires publics ou privés.

Analysis of Compressing PAPR-Reduced OFDM IQ Samples for Cloud Radio Access Network

Aya Shehata¹, Philippe Mary¹, *Member, IEEE*, and Matthieu Crussière¹, *Member, IEEE*

Abstract—A common problem of the virtualized cloud radio access network architecture (C-RAN) is the compression of the time-domain IQ samples before transmission over the fronthaul link. Considering a multicarrier waveform such as OFDM, whose IQ samples follow a quasi-Gaussian distribution, the conventional Gaussian quantizer may be used as the optimal solution to the compression problem. However, since the high peak-to-average power ratio (PAPR) of OFDM signals remains a serious problem, various techniques may be employed to reduce the time-domain fluctuations of the IQ samples in the OFDM, resulting in a change in its distribution. The latter fact makes the Gaussian quantizer suboptimal. The literature lacks a performance analysis of the conventional OFDM-based compression techniques when the PAPR of the OFDM signal is reduced. Therefore, in this paper, we study for the first time the impact of reducing the PAPR of the OFDM signal before compression in the C-RAN architecture through rate-distortion analysis. We consider clipping and tone reservation PAPR reduction algorithms. The former is the simplest PAPR reduction approach, while the latter is one of the most effective algorithms used in broadcasting standards such as DVB-T2 and ATSC 3.0. We first derive the distribution of the PAPR-reduced OFDM IQ samples. This is used to optimize the thresholds and codebook levels of a non-uniform scalar quantizer and the number of quantization bits allocated for each quantized level in the entropy coding stage, along with the MER performance analysis. The simulation results show that the conventional Gaussian-based compression techniques applied to a PAPR-reduced signal is not very robust to the statistical changes in the signal unless the signal distribution at the input of the Gaussian quantizer is not significantly affected. However, a significant gain is obtained when the quantizer is optimized with respect to the true distribution of the PAPR-reduced IQ samples.

Index Terms—C-RAN, clipping, compression, quantization, entropy coding, MER, OFDM, PAPR reduction, tone reservation, DVB-T2, ATSC3.0.

I. INTRODUCTION

NEXT generation wireless networks have recently adopted the promising architecture of the centralized Cloud Radio Access Network (C-RAN). The C-RAN architecture is based on splitting the base station functionalities into two parts, the baseband unit, located in the cloud, and the remote radio unit, located on transmission sites, and connecting them by a fronthaul link responsible for conveying the digitized

IQ samples [1], [2]. The fully centralized solution of such an architecture implies moving the physical layer including baseband processing and network layer functionalities to the cloud [3]. It provides high flexibility, low maintenance and operational cost. However, the huge bandwidth requirement for the transmission of high-resolution IQ samples generated by the baseband processing in the cloud remains a major problem of this architecture. The classical approach is to use higher bandwidth optical fibers to transport the IQ samples, but this comes at a very high cost. Therefore, IQ data compression before transmission over the capacity-constrained fronthaul link is an attractive approach to reduce the data rate over the fronthaul link for the C-RAN architecture.

Orthogonal frequency division multiplexing (OFDM) is the most commonly used multicarrier modulation scheme in recent standards, e.g., Long-term Evolution (LTE) [4], Digital Video Broadcasting-Second Generation Terrestrial (DVB-T2) [5], and Advanced Television Systems Committee 3.0 (ATSC3.0) standard [6]. Therefore, recent studies mainly rely on exploiting the statistical characteristics of the OFDM signal to reduce the data rate on the fronthaul link.

In recent years, several data rate compression approaches have been studied to represent the trade-off between achievable compression performance, signal distortion, design complexity and computational delay, which are summarized in [7], [8]. In [9], a non-uniform quantizer based on an iterative gradient algorithm was proposed. In [10], a Lloyd-based non-uniform quantizer and entropy coding were used to reduce the data rate of the fronthaul link. Vector quantization combined with decimation and block scaling was explored instead of scalar quantization to take advantage of the temporal correlation between IQ samples and increase the compression gain, but at the cost of higher computational complexity [11], [12]. In [13], the correlation between samples is explored through the well-known linear predictive coding to solve the complexity problem posed by vector quantization. In [14], trellis coded quantization has been implemented, which provides better compression performance than scalar quantization and lower computational cost than vector quantization. In [15], a discrete cosine transform (DCT) based compression scheme has been proposed. The DCT is a Fourier-dependent time-frequency transform characterized by its strong energy compaction property. Therefore, after DCT, the signal can be represented by coefficients in the frequency-domain, which can be divided into blocks of high and low frequency components. On this basis, the conventional compression methods, e.g., Lloyd-Max quantization and Huffman coding, are used to quantize and

Manuscript received December 17, 2021; revised March 4, 2022; accepted April 27, 2022. This work was supported by the BPIfrance for the FUI25 CLOUDCAST Project. This paper has been presented in part at IEEE PIMRC2021 [DOI: 10.1109/PIMRC50174.2021.9569447]. (*Corresponding author: Aya Shehata.*)

The authors are with the Univ Rennes, INSA Rennes, CNRS, IETR-UMR 6164, 35000 Rennes, France (e-mail: ayahanyshhata@gmail.com).

Digital Object Identifier 10.1109/TBC.2022.3176198

encode the high-frequency components with a smaller number of bits and the low-frequency components with more bits. In general, quantization and entropy coding are the main techniques to reduce the IQ data rate.

However, the addition of many subcarriers via the IFFT results in a signal characterized by a high peak-to-average power ratio (PAPR), which remains one of the main problems of the OFDM system. The high peak power of the signal leads to severe performance degradation when the signal is passed through a high power nonlinear amplifier. Many techniques have been presented in the literature that are applied to OFDM signal in the time-domain to reduce its PAPR, e.g., [16, and references therein].

In this paper, clipping and tone reservation (TR) PAPR reduction techniques are considered. Clipping is the simplest technique for PAPR reduction that provides a high reduction gain, although it results in signal distortion [17]. TR is an efficient method for PAPR reduction that has been adopted by several standards, e.g., DVB-T2 [5] and ATSC 3.0 [6], and it gives an upper bound on the PAPR reduction without distortion [18]. The concept of the TR algorithm is to dedicate a subset of the subcarriers, called the peak reserved tones (PRT), to change the OFDM signal distribution to another with a lower PAPR. This subset of reserved tones is loaded with complex values and added to the original signal, resulting in a transmitted time-domain signal with reduced PAPR. The symbols modulating the PRTs are the solutions of a convex quadratically constrained quadratic problem (QCQP). Many researchers have investigated a solution to the PRTs allocation problem in a suboptimal but simpler way [19, and references therein]. The major drawback of the optimal QCQP solution of the TR algorithm is its high complexity. However, adopting the C-RAN architecture increases the acceptability of the complexity of the QCQP solution by moving the implementation to the cloud.

Thanks to the central limit theorem, OFDM IQ samples are generally assumed to be Gaussian distributed at the output of the IFFT modulator. Therefore, the compression blocks, i.e., quantization and entropy coding, are optimized for a Gaussian distribution. However, processing the OFDM signal in the time-domain with a PAPR reduction technique changes the distribution of the IQ samples. To the best of our knowledge, no studies have been conducted on the robustness of the Gaussian-optimized quantizer considering any of the PAPR reduction techniques prior to compression, nor on the proposal of an optimized quantizer for signals with modified distribution due to PAPR reduction techniques. In this context, we have presented in a recent study the analytical analysis of the optimized quantizer and entropy coding for OFDM signals processed by the clipping algorithm [20]. In addition to our previous work, we include the study for signals processed by the QCQP algorithm. Hence, the contributions of this article can be summarized as follows:

- The distribution of PAPR-reduced IQ samples is derived and validated, taking into account clipping and TR obtained with the optimal QCQP solution. These analysis are based on recent studies that evaluate the amplitude distribution of the PAPR-reduced OFDM signal in the

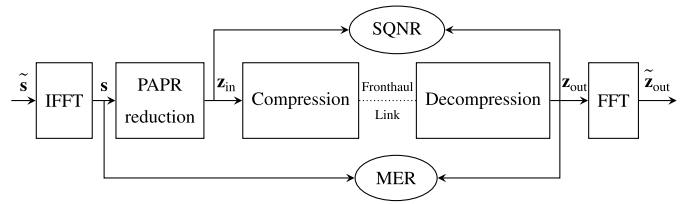


Fig. 1. Downlink system model of a C-RAN system.

case of clipping and TR-QCQP algorithms, [21] and [22], respectively.

- The obtained IQ distribution is further exploited to optimize the compression blocks, i.e., quantization and entropy coding, and to obtain an asymptotic expression for the modulation error ratio (MER), which reflects the joint effect of PAPR reduction and quantization operations.
- The robustness of a Gaussian-optimized quantizer to a change in the signal distribution at its input is investigated.
- Based on these analysis, we quantify the performance gain in MER when using a quantizer optimized with respect to the true distribution of PAPR-reduced IQ samples based on various tuning factors of the clipping and TR-QCQP algorithms compared to the Gaussian-based quantizer.

The remainder of this article is organized as follows. Section II describes the system model and revisits the recent state of the art, which evaluates the effect of PAPR reduction in changing the amplitude distribution of the OFDM signal. Section III details the analytical IQ distribution of the PAPR-reduced signal in case of clipping and TR-QCQP, and they are used to optimize the compression techniques. Section IV validates the accuracy of the theoretical findings through numerical simulations. Moreover, the gain in MER achieved by the PAPR-reduced optimized compression techniques is highlighted. Conclusions are drawn in Section V.

II. SYSTEM MODEL

A. OFDM Transmission Chain

Let us consider the downlink OFDM transmission chain depicted in Fig. 1. An OFDM system with N_{fft} subcarriers and M -QAM modulation is considered. A PAPR reduction technique is applied to the OFDM signal in the time-domain at the output of the IFFT modulator and then compressed before being transmitted over the fronthaul link. Let, in the time-domain, $\mathbf{s} \in \mathbb{C}^{N_{\text{fft}} \times 1}$ be the original complex OFDM baseband signal vector, with its k th entry expressed as

$$s(k) = \frac{1}{\sqrt{N_{\text{fft}}}} \sum_{n=0}^{N_{\text{fft}}-1} \tilde{s}(n) e^{j2\pi k \frac{n}{N_{\text{fft}}}}, \quad \forall k = [0, \dots, N_{\text{fft}} - 1] \quad (1)$$

where, $\tilde{\mathbf{s}} = [\tilde{s}(0), \dots, \tilde{s}(N_{\text{fft}} - 1)]^T \in \mathbb{C}^{N_{\text{fft}} \times 1}$ is a vector of QAM symbols modulating the subcarriers. In Fig. 1, the vector $\mathbf{z}_{\text{in}} \in \mathbb{C}^{N_{\text{fft}} \times 1}$ is the PAPR-reduced IQ samples before the compression and $\mathbf{z}_{\text{out}} \in \mathbb{C}^{N_{\text{fft}} \times 1}$ after the decompression. For N_{fft} sufficiently large, the real and imaginary parts

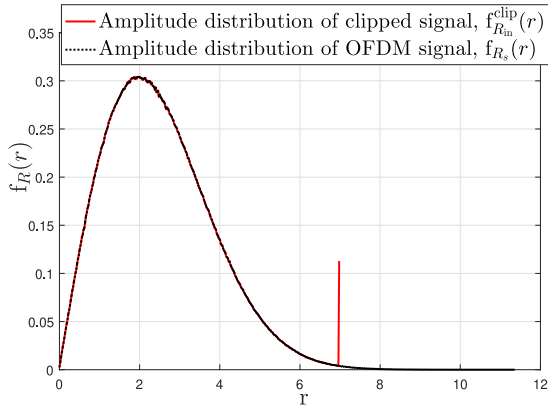


Fig. 2. PDF of the amplitude of the time-domain signal with and without clipping at $V_{\max} = 7$.

of a complex sample $s(k)$, $\forall k \in \{0, \dots, N_{\text{fft}} - 1\}$, denoted by $x_s(k) = \text{Re}(s(k))$ and $y_s(k) = \text{Im}(s(k))$, respectively, are zero-mean Gaussian distributed. Hence, its magnitude $r_s(k) = |s(k)|$ is Rayleigh distributed and its phase $\theta_s(k) = \angle s(k)$ is uniformly distributed over $[-\pi, \pi]$.

B. PAPR Reduction Techniques

1) *Clipping*: Clipping consists in limiting the high amplitude peaks of the signal to a certain threshold V_{\max} without affecting the phase of the signal. The clipped time-domain signal $z_{\text{in}}^{\text{clip}}(k)$ is given by:

$$z_{\text{in}}^{\text{clip}}(k) = \begin{cases} s(k), & \text{if } |s(k)| < V_{\max} \\ V_{\max} e^{j\theta_s}, & \text{if } |s(k)| \geq V_{\max}. \end{cases} \quad (2)$$

The amplitude of the signal at the input of the clipper is Rayleigh distributed

$$f_{R_s}(r) = \begin{cases} \frac{r}{\sigma_{\text{ray}}^2} e^{-\frac{r^2}{2\sigma_{\text{ray}}^2}}, & \text{if } r \geq 0 \\ 0, & \text{otherwise,} \end{cases} \quad (3)$$

where R_s is the random variable (RV) representing the amplitude of the input signal and σ_{ray} is its mode. The clipping ratio is defined as $\Lambda = \frac{V_{\max}^2}{2\sigma_{\text{ray}}^2}$. Clipping is applied on the signal amplitude as per (2) and it simply modifies the amplitude distribution as reminded in the following lemma.

Lemma 1 [21]: The time-domain amplitude distribution of the clipped PAPR-reduced signal, is expressed as follows:

$$f_{R_{\text{in}}}^{\text{clip}}(r) = \begin{cases} f_{R_s}(r), & \text{if } r < V_{\max} \\ e^{-\Lambda} \delta(r - V_{\max}), & \text{if } r = V_{\max} \end{cases} \quad (4)$$

where R_{in} is the RV representing the amplitude of the PAPR-reduced signal, $\delta(r)$ is the Dirac distribution and $e^{-\Lambda}$ is the probability that the amplitude of s exceeds V_{\max} , i.e., $\int_{V_{\max}}^{\infty} f_{R_s}(r) dr = e^{-\Lambda}$.

Fig. 2 depicts both distributions $f_{R_s}(r)$ and $f_{R_{\text{in}}}^{\text{clip}}(r)$. Clipping is simple but it may cause high signal distortion.

2) *Tone Reservation*: TR technique reduces the signal PAPR by adding a time-domain peak cancellation signal $\mathbf{c} \in \mathbb{C}^{N_{\text{fft}} \times 1}$ to the original OFDM signal \mathbf{s} . Thus, the tone-reserved

PAPR-reduced signal $\mathbf{z}_{\text{in}}^{\text{TR}}$ is expressed as follows:

$$z_{\text{in}}^{\text{TR}}(k) = s(k) + c(k), \quad \forall k = [0, \dots, N_{\text{fft}} - 1]. \quad (5)$$

Let $\tilde{\mathbf{c}}$ be the frequency-domain vector consisting of N_{fft} subcarriers composed of m tones reserved for peak reduction. These tones belong to the subset \mathcal{B} such that $\mathcal{B} = \{k \in [0, \dots, N_{\text{fft}} - 1] : \tilde{s}(k) = 0\}$ and $\mathcal{B}^c = \{k \in [0, \dots, N_{\text{fft}} - 1] : \tilde{c}(k) = 0\}$. Thus, $\tilde{\mathbf{s}}$ and $\tilde{\mathbf{c}}$ lie in disjoint frequency subspaces, which ensures that the TR technique is a distortion-less process. The concept of TR is to design an efficient algorithm capable of computing the peak cancellation signal \mathbf{c} in such a way that there is a trade-off between PAPR reduction efficiency and computational complexity.

The PAPR reduction efficiency of the TR algorithm is evaluated by two main tuning factors, namely the percentage of subcarriers dedicated for PAPR reduction out of the total number of subcarriers, denoted by N_{PRT} and the power allocated to PRTs. Typically, standards such as DVB-T2 add a peak power constraint to PRTs, denoted by P_{PRT} , to limit the power dedicated to PAPR reduction compared to the power of data tones, denoted by P_{data} . Let P_{PC} be the power control in dB, which denotes the difference between the maximum PRT power and the average data power. Thus, the power constraint condition can be mathematically expressed as follows [18]:

$$\max_{n \in \beta} \|\tilde{c}(n)\|_{\infty}^2 \leq \Gamma \cdot P_{\text{data}}, \quad (6)$$

where $\|\cdot\|_{\infty}$ denotes the infinity norm, $\Gamma = 10^{\frac{P_{\text{PC}}}{10}}$ and $P_{\text{PRT}} = \Gamma \cdot P_{\text{data}}$. The TR optimization problem can be formulated and solved optimally as a QCQP convex problem defined as [18]:

$$\begin{aligned} \min_{\mathbf{c}} \quad & \tau \\ \text{subject to} \quad & \|\mathbf{x} + \mathbf{c}\|_{\infty}^2 \leq \tau, \end{aligned} \quad (7)$$

where τ is the maximum power of \mathbf{z}_{in} . For cases considering a power constraint on the PRTs, as in DVB-T2 and ATSC3.0 for instance, (6) is added as an additional constraint to (7). QCQP solution achieves the highest PAPR reduction level but at a high computational complexity.

TR modifies the amplitude distribution of the OFDM signal. The authors in [22] evaluated the amplitude distribution of the tone-reserved signal solved by the optimal QCQP algorithm. They have shown that it is possible to model the amplitude distribution as a superposition of two separate modes, which is stated in the following lemma.

Lemma 2 [22]: The time-domain amplitude distribution of the tone-reserved PAPR-reduced signal, is expressed as follows:

$$f_{R_{\text{in}}}^{\text{QCQP}}(r) = (1 - p) f_{R_{\text{in}1}}(r) + p f_{R_{\text{in}2}}(r), \quad (8)$$

where

$$f_{R_{\text{in}1}}(r) = \begin{cases} q f_R^{\text{Ray}}(r) (1 - F_R^{\text{GEV}}(r)), & \text{if } r \geq 0 \\ 0, & \text{if } r < 0, \end{cases} \quad (9)$$

and

$$f_{R_{\text{in}2}}(r) = \begin{cases} f_R^{\text{GEV}}(r), & \text{if } r \in D_2 \\ 0, & \text{otherwise} \end{cases} \quad (10)$$

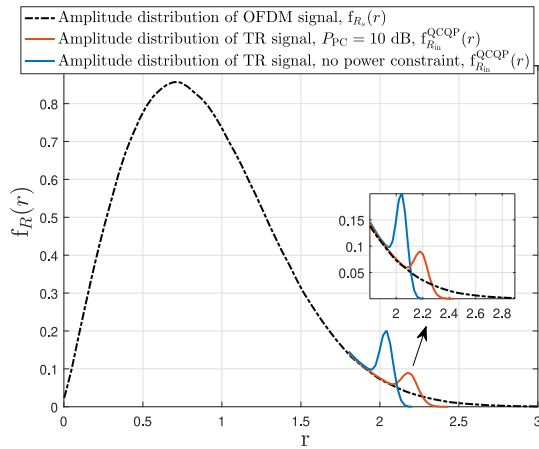


Fig. 3. PDF of the amplitude of the time-domain signal with and without TR-QCQP, with different power controls and $N_{\text{PRT}} = 1\%$.

where $R_{\text{in}1}$ and $R_{\text{in}2}$ are the RVs representing the samples drawn from the first and the second modes, respectively, p is a scaling parameter between the first and the second mode and q is a normalization parameter that ensures $\int f_{R_{\text{in}1}}(r)dr = 1$. $f_R^{\text{Ray}}(r)$, $F_R^{\text{GEV}}(r)$ and $f_R^{\text{GEV}}(r)$ are the Rayleigh PDF, the generalized extreme value (GEV) cumulative distribution function (CDF) and the GEV PDF, defined respectively as follows:

$$f_R^{\text{Ray}}(r) = \begin{cases} \frac{r}{\sigma_{\text{ray}}^2} e^{-\frac{r^2}{2\sigma_{\text{ray}}^2}}, & \text{if } r \geq 0 \\ 0, & \text{otherwise,} \end{cases} \quad (11)$$

$$F_R^{\text{GEV}}(r) = \begin{cases} e^{-\left(1+k_1\left(\frac{r-\mu_1}{\sigma_1}\right)\right)^{-1/k_1}}, & \text{if } r \in D_1 \\ 0, & \text{otherwise,} \end{cases} \quad (12)$$

and

$$f_R^{\text{GEV}}(r) = \begin{cases} \frac{1}{\sigma_2} t(r)^{k_2+1} e^{-t(r)}, & \text{if } r \in D_2 \\ 0, & \text{otherwise} \end{cases} \quad (13)$$

$$\text{with } t(r) = \left(1 + k_2 \left(\frac{r - \mu_2}{\sigma_2}\right)\right)^{-1/k_2}, \quad (14)$$

where σ_{ray} is the standard deviation fitting the Rayleigh distribution, $\mu_1, \sigma_1, k_1 < 0, \mu_2, \sigma_2$ and $k_2 < 0$ are respectively the location, scale and shape parameters that fit the GEV CDF $F_R^{\text{GEV}}(r)$ and the PDF $f_R^{\text{GEV}}(r)$, respectively and $D_1 =] - \infty, \mu_1 - \frac{\sigma_1}{k_1}]$ and $D_2 =] - \infty, \mu_2 - \frac{\sigma_2}{k_2}]$ are their respective domains.

The parameters of the Rayleigh and GEV distributions are computed in [22] using probability weighted moments estimation method. Fig. 3 shows the amplitude distributions of the OFDM signal before and after TR-QCQP, i.e., $f_{R_{\text{in}}}^{\text{Ray}}(r)$ and $f_{R_{\text{in}}}^{\text{QCQP}}(r)$, respectively. As already mentioned, the $f_{R_{\text{in}}}^{\text{QCQP}}(r)$ PDF can be modeled with a bimodal distribution whose parameters depend on the power control P_{PC} . The QCQP algorithm modifies the signal in such a way that the high amplitude samples has a lower probability to appear, compared to Rayleigh distributed samples. By doing so, QCQP concentrates the high amplitude samples to some levels that can be quantized without additional distortion. This results in a bump at the tail of the Rayleigh distribution, while the other samples still follow a Rayleigh amplitude distribution.

C. Compression Techniques

1) *Scalar Quantization*: Each IQ sample is quantized separately to one of N quantization levels, each represented by R quantization bits. The well-known Lloyd algorithm (LA) gives a scalar N -level non-uniform quantizer (NUQ), optimized in the sense of the minimum mean square error (MSE) for a given distribution of samples [23]. According to LA, decision thresholds $t_i, \forall i = [1, \dots, N-1]$ are

$$t_i = \frac{q_i + q_{i+1}}{2}, \quad (15)$$

where, t_0 and t_N are set to the minimum and maximum possible values of the signal, respectively. Quantization levels $q_i, \forall i = [1, \dots, N]$, are the centroid of each decision region, e.g., for the in-phase component

$$q_i = \frac{\int_{t_{i-1}}^{t_i} x f_X(x) dx}{\int_{t_{i-1}}^{t_i} f_X(x) dx}, \quad (16)$$

where $f_X(x)$ is the PDF associated to the in-phase component $x(k) = \text{Re}(z_{\text{in}}(k)), \forall k$, of the PAPR-reduced signal. The same holds for the Quadrature-phase component.

2) *Entropy Coding*: Entropy coding (EC) is a lossless compression technique. It generates variable length codewords by assigning longer codewords to the lower probability levels and shorter codewords to the higher probability levels. In this paper, Huffman coding is used in order to reduce the amount of bits transmitted over the fronthaul. It is a well-known, simple method for practical implementation of entropy coding and that approaches the Shannon's source coding theorem [24]. Thus, the average codeword length assigned to the i th quantization level can be represented with the information entropy as

$$L_{q_i} = -\log_2 \int_{t_{i-1}}^{t_i} f_X(x) dx. \quad (17)$$

D. Performance Metrics

The Rate R , MER and signal to quantization and noise ratio (SQNR) are the metrics used to evaluate the performance of the model under study. In this context, R is defined as the average number of bits required to represent a single IQ sample.

1) *MER*: The MER gives a measure of the performance of the system by comparing the actual location of a received sample with its ideal location. It is defined as the ratio between the power of the original signal and the distortion introduced to the original signal. Therefore, the MER of the decompressed signal is defined as

$$\text{MER} = \frac{\mathbb{E}[|S|^2]}{\mathbb{E}[|S - Z_{\text{out}}|^2]}, \quad (18)$$

with $\mathbb{E}[\cdot]$ is the expectation operator, S and Z_{out} are the RVs representing the IQ samples before the compression and after decompression, respectively.

2) *SQNR*: The SQNR is used to evaluate the performance of the compression achieved by quantization, since EC is indeed distortion-less. In this case, \mathbf{z}_{in} is considered as the reference signal and the SQNR is defined as

$$\text{SQNR} = \frac{\mathbb{E}[|Z_{\text{in}}|^2]}{\mathbb{E}[|Z_{\text{in}} - Z_{\text{out}}|^2]}, \quad (19)$$

where Z_{in} is the RV representing the PAPR-reduced samples. In that perspective, the following facts need to be considered for proper system evaluation.

- In case of clipping PAPR reduction technique, both clipping and quantization operations contribute to system performance degradation.
- In TR PAPR reduction technique, the received signal $\tilde{\mathbf{z}}_{\text{out}}$ is followed by removing the TR added signal, thanks to the orthogonality between the data and the tone-reserved signals in the frequency-domain. Thus, the distortion induced to the OFDM signal is caused only by the quantization. Consequently, the MER can be evaluated between \mathbf{s} and \mathbf{z}_{out} after removing the added TR signal in the frequency-domain or between the intermediate signals \mathbf{z}_{in} and \mathbf{z}_{out} . We will consider the latter case, where the system MER can be computed directly from (19), taking into account only the quantization distortion.
- The MSE in the denominator of (19) indicates the quantization distortion. Through our analytical analysis, we consider the asymptotic (high bit-rate) quantization distortion stated as follows.

Proposition 1 [25]: The asymptotic distortion-rate formula for a non-uniform scalar quantizer is known as “*Panter and Dite formula*” and stated as:

$$D_{\text{LQ}}(R) \sim \frac{2^{-2R}}{12} \left(\int_{-\infty}^{\infty} \sqrt[3]{f_X(x)} dx \right)^3. \quad (20)$$

where $f_X(x)$ is the PDF of the quantizer input signal, $R = \log_2(N)$ and N is the number of quantization levels.

III. ANALYTICAL STUDY OF THE OPTIMIZED COMPRESSION TECHNIQUES FOR A PAPR-REDUCED SIGNAL

The optimization of a Lloyd-based quantizer may be led using either a known probabilistic distribution or an observed long training sequence (TS) of data. The main drawbacks of the latter is

- An N -level quantizer trained on a k -length TS requires computing $N.k$ distances and assigning k data points at each iteration until convergence.
- A sufficiently long TS is essential so that the resulting quantizer hopefully works well for future data.
- The algorithm must be repeated multiple times with different initial TS to mitigate dependence.

Such intensive computations make Lloyd’s algorithm slow, especially for large datasets. Therefore, prior knowledge of the probabilistic description of the source is more efficient and requires less computational complexity. On the other hand, Huffman coding suffers from a deviation from the entropy bound when the statistical property of the source is unknown.

Therefore, in this section, we first derive the distribution of the PAPR-reduced IQ samples, i.e., $f_X(x)$ and $f_Y(y)$ for the In-phase and Quadrature-phase components, respectively. The parameters of the NUQ and EC blocks for the new distribution of the signal with reduced PAPR are analyzed and consequently the joint effect of PAPR reduction and compression distortion is modeled by MER analysis.

A. Distribution of the PAPR-Reduced IQ Samples

The conversion from polar to Cartesian coordinates of the complex samples is such that $(x, y) = \varphi(r, \theta)$ with:

$$\begin{aligned} x &= r \cos \theta & r &= \sqrt{x^2 + y^2} \\ y &= r \sin \theta & \theta &= \varphi_2^{-1}(x, y), \end{aligned} \quad (21)$$

where $\varphi : \zeta \mapsto \Delta$ is a one-to-one mapping from the polar coordinates domain ζ to the Cartesian coordinates domain Δ and $\varphi_2^{-1} : \Delta \mapsto [-\pi, \pi]$ with:

$$\varphi_2^{-1}(x, y) = \begin{cases} \tan^{-1}\left(\frac{y}{x}\right), & \text{if } x > 0 \\ \tan^{-1}\left(\frac{y}{x}\right) - \pi, & \text{if } x < 0, y < 0 \\ \pi - \tan^{-1}\left(\frac{y}{x}\right), & \text{if } x < 0, y \geq 0 \\ \pi/2, & \text{if } x = 0, y > 0 \\ -\pi/2, & \text{if } x = 0, y < 0. \end{cases} \quad (22)$$

According to the change of variables theorem, the joint PDF of the couple (X, Y) is

$$f_{X,Y}(x, y) = |J(x, y)| f_{R_{\text{in}}, \Theta_{\text{in}}}(r(x, y), \theta(x, y)), \quad (23)$$

where $|J(x, y)|$ is the modulus of the Jacobian of the mapping φ computed as

$$|J(x, y)| = \left| \begin{vmatrix} \frac{\partial r}{\partial x} & \frac{\partial r}{\partial y} \\ \frac{\partial \theta}{\partial x} & \frac{\partial \theta}{\partial y} \end{vmatrix} \right| = \frac{1}{\sqrt{x^2 + y^2}}, \quad \forall (x, y) \neq (0, 0) \quad (24)$$

As reminded in Section II-B, the considered PAPR reduction techniques modify the signal amplitude without affecting the phase. Thus, $\forall k \in \{0, \dots, N_{\text{fft}} - 1\}$, $r_{\text{in}}(k) = |z_{\text{in}}(k)|$ and $\theta_{\text{in}}(k) = \angle z_{\text{in}}(k)$ are samples drawn from two independent random variables, i.e., R_{in} and Θ_{in} , respectively. Hence, the joint PDF of $(R_{\text{in}}, \Theta_{\text{in}})$ is the product of the marginal PDFs, i.e., $f_{R_{\text{in}}, \Theta_{\text{in}}}(r, \theta) = f_{R_{\text{in}}}(r) f_{\Theta_{\text{in}}}(\theta)$.

1) *Clipping*: The respective domains of the polar and Cartesian coordinates become $\zeta = [0, V_{\text{max}}] \times [-\pi, \pi]$ and $\Delta =]-V_{\text{max}}, V_{\text{max}}[^2$, respectively. Using the amplitude distribution of the clipped signal in Lemma 1, the joint PDF of the polar coordinates can be expressed as

$$f_{R_{\text{in}}, \Theta_{\text{in}}}^{\text{clip}}(r, \theta) = \begin{cases} \frac{r}{2\pi\sigma_{\text{ray}}^2} e^{-\frac{r^2}{2\sigma_{\text{ray}}^2}}, & \text{if } r < V_{\text{max}} \\ \frac{e^{-\Lambda}}{2\pi} \delta(r - V_{\text{max}}), & \text{if } r = V_{\text{max}}. \end{cases} \quad (25)$$

Thus, substituting (25) and (24) into (23), the marginal PDF of the Cartesian coordinate of a clipped RV is obtained as

$$f_X^{\text{clip}}(x) = \int_{-V_{\text{max}}}^{V_{\text{max}}} \left(\frac{1}{2\pi\sigma_{\text{ray}}^2} e^{-\frac{x^2+y^2}{2\sigma_{\text{ray}}^2}} + \frac{e^{-\Lambda}}{2\pi\sqrt{x^2+y^2}} \times \delta\left(\sqrt{x^2+y^2} - V_{\text{max}}\right) \right) dy. \quad (26)$$

Thus, a closed-form expression of the PDF of the clipped IQ samples can be obtained as in the following theorem.

Theorem 1: The probability distribution of the clipped PAPR-reduced IQ samples after IFFT, is expressed as follows:

$$f_X^{\text{clip}}(x) = \frac{1}{\sqrt{2\pi}\sigma_{\text{ray}}} e^{-\frac{x^2}{2\sigma_{\text{ray}}^2}} \operatorname{erf}\left(\frac{V_{\text{max}}}{\sqrt{2\sigma_{\text{ray}}^2}}\right) + \frac{e^{-\Lambda}}{2\pi} \frac{1}{\sqrt{V_{\text{max}}^2 - x^2}}, \quad x \in]-V_{\text{max}}, V_{\text{max}}[\quad (27)$$

where $\operatorname{erf}(u) = (2/\sqrt{\pi}) \int_0^u \exp(-t^2) dt$ is the error function.

Proof: Using the integral identity in [26, eq. (1), Sec. 3.321, p. 336] and applying the change of variable $z = \sqrt{x^2 + y^2}$, then adequately rearranging the terms leads to the given distribution of the In-phase component $f_X^{\text{clip}}(x)$. ■

From (27), one can check that without clipping, i.e., when $V_{\text{max}} \rightarrow \infty$ and hence $\Lambda \rightarrow \infty$, the second term vanishes and the error function tends to one. This leads to the zero-mean Gaussian distribution characterizing the OFDM signal.

2) *TR With QCQP Solution:* The respective domains of the polar and Cartesian coordinates are $\zeta = [0, \infty) \times [-\pi, \pi]$ and $\Delta = \mathbb{R}^2$. The joint PDF $f_{R_{\text{in}}, \Theta_{\text{in}}}^{\text{QCQP}}(r, \theta)$ is the product of the amplitude distribution of the TR-QCQP signal in Lemma 2 and the phase distribution $f_{\Theta_{\text{in}}}^{\text{QCQP}}(\theta) = \frac{1}{2\pi}$. Hence, Substituting the joint PDF in (23) together with the Jacobian determinant in (24), the marginal PDF of the Cartesian coordinate of the tone-reserved RV is obtained from

$$f_X^{\text{QCQP}}(x) = \underbrace{\int_{-\infty}^{\infty} \frac{(1-p)q}{2\pi\sigma_{\text{ray}}^2} e^{-\frac{x^2+y^2}{2\sigma_{\text{ray}}^2}} \left(1 - F_R^{\text{GEV}}(r(x, y))\right) dy}_{f_{X_1}(x)} + \underbrace{\int_{-\infty}^{\infty} \frac{p}{2\pi\sigma_2\sqrt{x^2+y^2}} G(x, y)^{k_2+1} e^{-G(x, y)} dy}_{f_{X_2}(x)} \quad (28)$$

$$\text{where, } F_R^{\text{GEV}}(r(x, y)) = e^{-\left(1 + \frac{k_1}{\sigma_1} (\sqrt{x^2+y^2} - \mu_1)\right)^{-1/k_1}}, \quad (29)$$

$$\text{and } G(x, y) = \left(1 + \frac{k_2}{\sigma_2} (\sqrt{x^2+y^2} - \mu_2)\right)^{-1/k_2}. \quad (30)$$

where X_1 and X_2 are the RVs representing the samples drawn from the first and the second mode of the In-phase Cartesian distribution, respectively. Finally, one can show that the distribution of the In-phase component, $f_X^{\text{QCQP}}(x)$,¹ can be expressed as in the following theorem.

Theorem 2: The probability distribution of the TR-QCQP PAPR-reduced IQ samples after IFFT, is expressed as follows:

$$f_X^{\text{QCQP}}(x) = f_{X_1}(x) + f_{X_2}(x), \quad x \in]-d^*, d^*[\quad (31)$$

where

$$f_{X_1}(x) = \frac{(1-p)q}{\sqrt{2\pi}\sigma_{\text{ray}}} e^{-\frac{x^2}{2\sigma_{\text{ray}}^2}} \operatorname{erf}\left(\frac{\sqrt{r_s^2 - x^2}}{\sqrt{2\sigma_{\text{ray}}^2}}\right) \quad (32)$$

¹The distribution of the Quadrature-phase component, $f_Y^{\text{clip}}(y)$ and $f_Y^{\text{QCQP}}(y)$, derives from the same steps as in Theorems 1 and 2, respectively, given that the phase is uniformly distributed.

$$\text{with } r_s = \mu_1 + \frac{\sigma_1}{k_1} \left((\ln 2)^{-k_1} - 1\right) \quad (33)$$

and

$$f_{X_2}(x) = \frac{-p}{\pi} \sum_{p_1=0}^{\infty} \sum_{p_2=0}^{p_1} \xi \left[\Gamma(k_2(p_1 + p_2 + 1) + 1, \psi_1) - \Gamma(k_2(p_1 + p_2 + 1) + 1, \psi_2) \right], \quad (34)$$

$$\text{with, } \xi = \binom{-\frac{1}{2}}{p_1} \binom{p_1}{p_2} \left[c_1^{-\frac{(1+2p_1)}{2}} c_2^{p_1-p_2} c_3^{p_2} \right], \quad (35)$$

$$\text{and } c_1 = \frac{\sigma_2^2}{k_2^2}, \quad c_2 = \frac{2\mu_2\sigma_2}{k_2} - 2c_1,$$

$$c_3 = -c_1 - c_2 + \mu_2^2 - x^2,$$

$$\psi_1 = \left[1 + \frac{k_2}{\sigma_2} (x - \mu_2) \right]^{-\frac{1}{k_2}},$$

$$\psi_2 = \left[1 + \frac{k_2}{\sigma_2} (\sqrt{x^2 + d^{*2}} - \mu_2) \right]^{-\frac{1}{k_2}}. \quad (36)$$

and

$$d^* = \max\left(r_s, \mu_2 - \frac{\sigma_2}{k_2}\right). \quad (37)$$

where $\Gamma(u, v) = \int_v^{\infty} e^{-t} t^{u-1} dt$ is the upper incomplete Gamma function, $\binom{r}{k}$ is the generalized binomial coefficient defined as $\binom{r}{k} = \frac{(r)_k}{k!}$ where, $(r)_k = \prod_{n=0}^{k-1} (r-n)$ is the falling factorial and $p, q, \sigma_{\text{ray}}, \mu_1, \sigma_1, k_1, \mu_2, \sigma_2$, and k_2 are the fitted parameters of the amplitude distribution $f_{R_{\text{in}}}^{\text{QCQP}}(r)$ in Lemma 2.

Proof: See Appendix A. ■

We can see that the distribution of the TR-QCQP IQ samples takes the form of a series expansion with gamma functions and depends on the estimated fitted parameters of the GEV and Rayleigh distributions, which model the amplitude of the tone-reserved signal in Lemma 2.

B. Derivation of Optimized Quantizer and EC Parameters

Based on the PDF of the clipped PAPR-reduced IQ samples in Theorem 1, the parameters of the optimized compression techniques can be derived by injecting this PDF into (16) and (17), as in the following proposition.

Proposition 2: The codebook quantization levels for the real and imaginary parts of a clipped signal and the average codeword length assigned to each quantization level in the entropy coder stage can be expressed by (38) and (39), respectively, on the bottom of the next page, where $Q(u) = (1/\sqrt{2\pi}) \int_u^{\infty} \exp(-v^2/2) dv$ is the Q-function.

Proof: Applying the adequate change of variables $u = \sqrt{V_{\text{max}}^2 - x^2}$ and $x = V_{\text{max}} \sin u$ for the numerator and the denominator of (16), respectively, along with the integral identity in [26, eq. (1), Sec. 3.321, p. 336], q_i^{clip} and $L_{q_i}^{\text{clip}}$ are obtained. ■

Without clipping, i.e., when $V_{\text{max}} \rightarrow \infty$ and hence $\Lambda \rightarrow \infty$, the error function tends to one and the exponential term in (38) and (39) tends to zero and we obtain the parameters of a quantizer and an entropy encoder, optimized for a zero-mean Gaussian distribution analyzed in [8]. The PDF of the tone-reserved IQ samples obtained in Theorem 2 remains complex because special functions with complex arguments are

involved. Therefore, closed form expressions for the codebook quantization levels and the average codeword length assigned to each quantization level are unattainable for PAPR-reduced signals with tone-reservation technique and they are computed numerically by injecting $f_X^{\text{QCQP}}(x)$ into (16) and (17), respectively.

C. Derivation of Asymptotic MER and SQNR

A closed-form expression of the MER and SQNR in (18) and (19), respectively, can be evaluated asymptotically for the clipping PAPR reduction technique based on Theorem 1 as stated in the following lemma. In that case, the asymptotic SQNR is only important to evaluate the distortion caused by the quantizer.

Lemma 3: The asymptotic MER and SQNR expressions of a compressed clipped OFDM signal, considering a scalar NUQ and EC can be expressed by:

$$\text{MER}^{\text{clip}} = \frac{P_s}{D_C + D_{\text{LQ}}^{\text{clip}}} = \frac{2\sigma_{\text{ray}}^2}{D_C + D_{\text{LQ}}^{\text{clip}}}, \quad (40)$$

and

$$\text{SQNR}^{\text{clip}} = \frac{P_{z_{\text{in}}}^{\text{clip}}}{D_{\text{LQ}}^{\text{clip}}}, \quad (41)$$

where D_C , $D_{\text{LQ}}^{\text{clip}}$ and $P_{z_{\text{in}}}^{\text{clip}}$ are the clipping distortion, asymptotic quantization distortion and the power of the complex clipped IQ samples, given in (43), (44) and (44) on the bottom of the page, respectively, where

$$a = \frac{1}{\sqrt{2\pi}\sigma_{\text{ray}}^2} \text{erf}\left(\frac{V_{\text{max}}}{\sqrt{2\sigma_{\text{ray}}^2}}\right), \quad b = \frac{1}{2\sigma_{\text{ray}}^2}, \quad \text{and} \quad c = \frac{e^{-\Lambda}}{2\pi}. \quad (42)$$

where ${}_1F_1$ is the confluent hypergeometric function [26, Sec. 9.18, p. 1019].

Proof: See Appendix B. ■

For TR-QCQP, the asymptotic MER of the compressed tone-reserved OFDM signal can be computed numerically from (18) based on the PDF of the tone-reserved IQ samples $f_X^{\text{QCQP}}(x)$ in Theorem 2. The numerator of (18) is the average power of a complex tone-reserved IQ sample, denoted by $P_{z_{\text{in}}}^{\text{QCQP}}$ and is calculated from $P_{z_{\text{in}}}^{\text{QCQP}} = 2 \int_{-d^*}^{d^*} x^2 f_X^{\text{QCQP}}(x) dx$. As shown earlier, quantization is the only source of distortion for the TR PAPR reduction technique. Therefore, the denominator of (18) is the quantization distortion asymptotically computed from Proposition 1.

D. Complexity Analysis

The algorithmic complexity of the proposed optimized compression techniques is the complexity of the Lloyd algorithm for non-uniform scalar quantizer [23]. This algorithm is a two-step iterative process satisfying the two optimality conditions given in (15) and (16). Each iteration requires to compute $N-1$ decision thresholds and N quantization levels, with $N = 2^R$, R being the number of bits, hence the complexity of an iteration is in $O(N)$. Iterations continue until the algorithm converges, i.e., when the quantization distortion does not improve anymore. The computations of the decision thresholds (15) and the codewords (16) depend on the PDF of the samples which is a bit more complex than for a strictly Gaussian signal. Indeed, for a clipped optimized quantizer, the quantization levels are computed from Proposition 2 with (38). For the tone-reserved optimized quantizer, quantization levels are numerically computed using Theorem 2 in (16), which is far more complex than computing a Gaussian quantizer. However, it is worth noting that these implementations are moved to the cloud in a

$$q_i^{\text{clip}} = \frac{\frac{\sigma_{\text{ray}}}{\sqrt{2\pi}} \text{erf}\left(\frac{V_{\text{max}}}{\sqrt{2\sigma_{\text{ray}}^2}}\right) \left[e^{-\frac{t_{i-1}^2}{2\sigma_{\text{ray}}^2}} - e^{-\frac{t_i^2}{2\sigma_{\text{ray}}^2}} \right] + \frac{e^{-\Lambda}}{2\pi} \left[\sqrt{V_{\text{max}}^2 - t_{i-1}^2} - \sqrt{V_{\text{max}}^2 - t_i^2} \right]}{\text{erf}\left(\frac{V_{\text{max}}}{\sqrt{2\sigma_{\text{ray}}^2}}\right) \left[Q\left(\frac{t_{i-1}}{\sigma_{\text{ray}}}\right) - Q\left(\frac{t_i}{\sigma_{\text{ray}}}\right) \right] + e^{-\frac{\Lambda}{2\sigma_{\text{ray}}^2}} \left[\arcsin\left(\frac{t_{i-1}}{V_{\text{max}}}\right) - \arcsin\left(\frac{t_i}{V_{\text{max}}}\right) \right]} \quad (38)$$

$$L_{q_i}^{\text{clip}} = -\log_2 \left(\text{erf}\left(\frac{V_{\text{max}}}{\sqrt{2\sigma_{\text{ray}}^2}}\right) \left[Q\left(\frac{t_{i-1}}{\sigma_{\text{ray}}}\right) - Q\left(\frac{t_i}{\sigma_{\text{ray}}}\right) \right] + e^{-\frac{\Lambda}{2\sigma_{\text{ray}}^2}} \left[\arcsin\left(\frac{t_{i-1}}{V_{\text{max}}}\right) - \arcsin\left(\frac{t_i}{V_{\text{max}}}\right) \right] \right) \quad (39)$$

$$D_C = 2\sigma_{\text{ray}}^2 \Gamma\left(2, \frac{V_{\text{max}}^2}{2\sigma_{\text{ray}}^2}\right) - 2^{\frac{3}{2}} \sigma_{\text{ray}} V_{\text{max}} \Gamma\left(\frac{3}{2}, \frac{V_{\text{max}}^2}{2\sigma_{\text{ray}}^2}\right) + V_{\text{max}}^2 e^{-\frac{V_{\text{max}}^2}{2\sigma_{\text{ray}}^2}} \quad (43)$$

$$D_{\text{LQ}}^{\text{clip}} = \frac{2^{-2R}}{6} \left[\frac{2\sqrt[3]{a}V_{\text{max}}}{\sqrt{6b\sigma_{\text{ray}}^2}} {}_1F_1\left(\frac{1}{2}; \frac{3}{2}; -\frac{V_{\text{max}}^2}{6\sigma_{\text{ray}}^2}\right) - \frac{26cV_{\text{max}}}{25\sqrt{3\sigma_{\text{ray}}^2}\sqrt[3]{a^2}} {}_1F_1\left(\frac{1}{2}; 1; \frac{V_{\text{max}}^2}{3\sigma_{\text{ray}}^2}\right) \right]^3 \quad (44)$$

$$P_{z_{\text{in}}}^{\text{clip}} = \frac{2\sigma_{\text{ray}}^2}{\sqrt{\pi}} \text{erf}\left(\frac{V_{\text{max}}}{\sqrt{2\sigma_{\text{ray}}^2}}\right) \left[\sqrt{\frac{\pi}{2}} \text{erf}\left(\frac{V_{\text{max}}}{\sqrt{2\sigma_{\text{ray}}^2}}\right) - \frac{V_{\text{max}}}{\sqrt{2\sigma_{\text{ray}}^2}} e^{-\frac{V_{\text{max}}^2}{2\sigma_{\text{ray}}^2}} \right] + \frac{V_{\text{max}}^2}{4} e^{-\frac{V_{\text{max}}^2}{2\sigma_{\text{ray}}^2}} \quad (45)$$

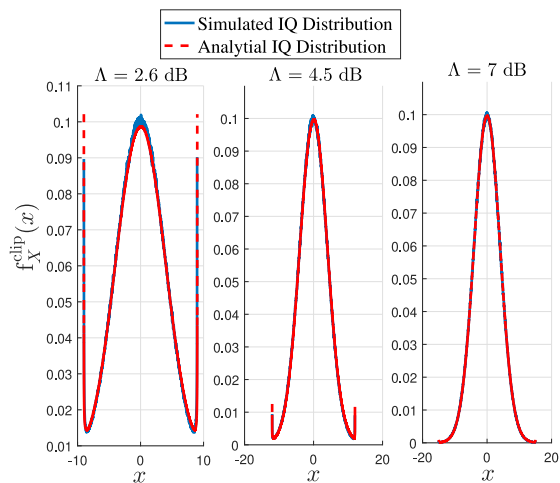


Fig. 4. Simulated and analytical PDF of clipped PAPR-reduced IQ samples for different clipping ratios Λ .

CRAN architecture in which the complexity is a less stringent constraint than in radio heads.

IV. RESULTS ANALYSIS

This section validates through simulations the distributions of the IQ samples obtained after clipping and tone-reservation techniques derived in Theorems 1 and 2, respectively. These expressions are then exploited to analyze the effect of reducing the PAPR of the OFDM signal before compression in a C-RAN architecture.

In our simulations, without loss of generality, we consider an 8-MHz DVB-T2 frame structure with 64-QAM constellations.² The 32k FFT mode is considered for the analysis of the clipping PAPR reduction technique with 32768 active subcarriers conveying the QAM symbols. On the other hand, only the 8k mode with 8192 subcarriers is considered for TR-QCQP due to the prohibitive computational complexity of QCQP for larger FFT sizes. It can be emphasised that an N_{fft} size of 8k is sufficiently large to ensure the convergence of the real and imaginary parts of the complex OFDM signal to a Gaussian distribution. This ensures a fair comparison between the clipping and TR analysis. In TR, when analyzing the impact of the different power control P_{PC} applied to PRT subcarriers compared to data subcarriers, we set a percentage of dedicated subcarriers $N_{\text{PRT}} = 1\%$ and the PRT positions are those used in the DVB-T2 frame structure. While, in case of a different percentage of subcarriers dedicated for the TR algorithm N_{PRT} , we set a power control $P_{\text{PC}} = 10$ dB and randomly generate the positions of the PRTs.

A. Distribution of the PAPR-Reduced IQ Samples

1) *Clipping*: We start by validating the obtained clipped PAPR-reduced IQ samples PDF in Theorem 1. Fig. 4 shows the PDF for different clipping ratios of 2.6 dB, 4.5 dB, and

²Note that the order of the constellations has a very limited impact on the distribution of the samples in the time-domain. Hence, simple 64-QAM is used in the simulation instead of more sophisticated constellation such as rotated 256-QAM, which is used in DVB-T2 and ATSC3.0 for instance.

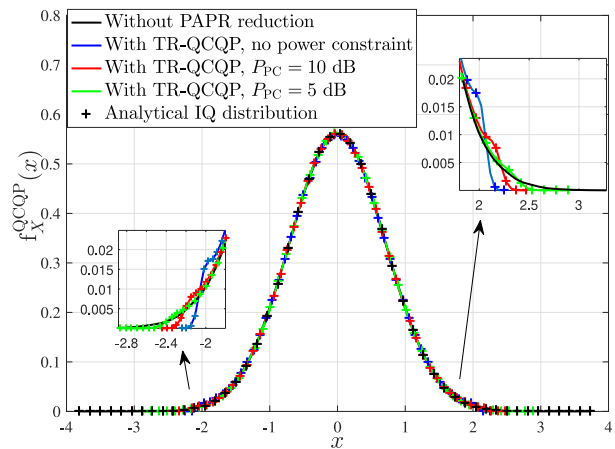


Fig. 5. Simulated and analytical PDF of TR-QCQP PAPR-reduced IQ samples, with and without power constraint and $N_{\text{PRT}} = 1\%$.

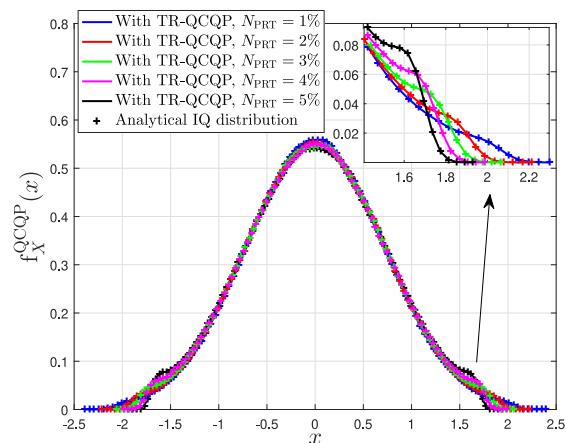


Fig. 6. Simulated and analytical PDF of TR-QCQP PAPR-reduced IQ samples, with different percentages of reserved tones and $P_{\text{PC}} = 10$ dB.

7 dB, respectively. The analytical curves perfectly match the simulated ones, which validates the obtained statement in Theorem 1. It is worth noting that the distribution of the clipped IQ samples converges to a zero-mean Gaussian distribution when increasing the clipping threshold. Indeed, as the clipping threshold increases, the distortion decreases as expected from (27).

2) *TR With QCQP Solution*: We validate the distribution of the TR-QCQP PAPR-reduced IQ samples expressed in Theorem 2. Fig. 5 shows the analytical³ and the simulated IQ PDF for a set of 1% PRT over the total number of subcarriers. The power constraint applied to PRT subcarriers compared to data subcarriers is set to 5, 10 dB or no constraint. Moreover, in Fig. 6, the simulated and analytical PDF are shown for different percentages of reserved tones over the total number of subcarriers and with a power constraint $P_{\text{PC}} = 10$ dB. It is important to mention that the TR algorithm introduces a power increase on reserved subcarriers compared to data subcarriers, according to the power constraint defined in (6). Thus, in order to ensure a fair comparison, the energy of the tone-reserved

³We use the fitted parameters of the amplitude distribution of the TR-QCQP signal estimated in [22].

PAPR-reduced signals is normalized to 1. Finally, our findings in Theorem 2 are perfectly validated by Figures 5 and 6. For our upcoming analysis, it is important to investigate how the distribution of the tone-reserved IQ samples depends on the tuning factors P_{PC} and N_{PRT} .

a) *Impact of power control P_{PC}* : The distribution of the signal before applying the tone-reservation algorithm is Gaussian, as observed in Fig. 5. On the other hand, the PDF after TR is a multimodal distribution with a major mode and two minor modes taking the form of “shoulders” on each side of the main mode. The probability of the minor modes is very small compared to the main mode and depends on the value of the power control P_{PC} . The main mode still follows a Gaussian distribution at small signal values, and the power assigned to the PRTs allows the tail of the distribution to change as follows. When additional power is added, the tail of the distribution decreases and the concentration of the minor mode becomes more significant. More precisely, when no power constraint is applied, the tail of the distribution is reduced as much as possible.

b) *Impact of percentage of PRTs*: The larger the number of reserved tones, the more the PAPR is reduced. Therefore and as previously, the tail of the distribution decreases, along with the growth of the minor modes, when N_{PRT} increases, as observed in Fig. 6.

B. Distortion-Rate Analysis

In this section, we show the gain in the performance of the lossy compression technique, i.e., quantization, resulting from the change of the distribution of the OFDM signal when it is subjected to a PAPR reduction technique. These analysis are presented asymptotically based on Shannon distortion-rate theory. Shannon gave a fundamental lower bound (SLB) for the distortion-rate function, which indicates the minimum achievable distortion for a given rate $D^*(R)$ that should be considered in any lossy compression technique. SLB for a stationary identical and independently distributed (i.i.d) source and MSE distortion D is given by [27]

$$D^*(R) = \frac{1}{2\pi e} 2^{2h(X)} 2^{-2R}, \quad (46)$$

where e is the exponential and $h(X)$ is the differential entropy of an absolutely continuous RV X and is defined as

$$h(X) = - \int_{\mathcal{X}} f_X(x) \log_2 f_X(x) dx. \quad (47)$$

where \mathcal{X} is the set denoting the support of RV X . Although the distortion-rate function has a simple expression, it cannot be evaluated analytically except in a few special cases. However, it is well known that the Gaussian source maximizes the differential entropy and hence the SLB for a given variance [27]. Therefore, for a RV X with a given variance σ^2 , $h(X)$ is upper bounded by

$$h(X) \leq h_G(X) = \frac{1}{2} \log_2(2\pi e\sigma^2), \quad (48)$$

and the distortion-rate is in turn upper bounded as follows:

$$D^*(R) \leq D_G^*(R) = \sigma^2 2^{-2R}, \quad (49)$$

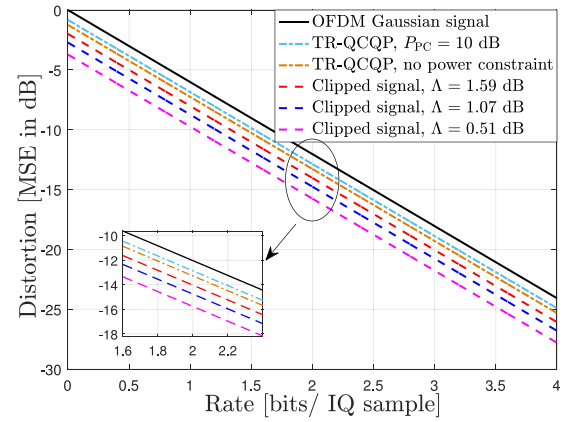


Fig. 7. $D_{\text{clip}}^*(R)$ and $D_{\text{QCQP}}^*(R)$ functions for clipped and TR-QCQP PAPR-reduced signals, at different Λ and P_{PC} , respectively, bounded above by the Gaussian distortion-rate function $D_G^*(R)$.

where $h_G(X)$ is the differential entropy of a Gaussian random variable with variance σ^2 and $D_G^*(R)$ is SLB for a Gaussian source.

Fig. 7 shows the distortion-rate Shannon bounds for clipped signals with different clipping ratios, denoted $D_{\text{clip}}^*(R)$, and for tone-reserved signals with different power constraints, denoted $D_{\text{QCQP}}^*(R)$, together with the Gaussian upper bound $D_G^*(R)$. The Gaussian upper bound $D_G^*(R)$ is plotted from (49), while the distortion-rate functions $D_{\text{clip}}^*(R)$ and $D_{\text{QCQP}}^*(R)$ are computed numerically using the corresponding PDFs in Theorems 1 and 2, respectively, in (46).

It can be seen that the highest distortion results from the Gaussian distribution. At low clipping ratios, the deviation of $D_{\text{clip}}^*(R)$ from the Gaussian $D_G^*(R)$ is clearly seen. As the clipping ratio increases and the signal converges to a zero-mean Gaussian distributed signal, this deviation decreases. Moreover, $D_{\text{QCQP}}^*(R)$ is slightly lower than the Gaussian upper limit. This is because the TR-QCQP algorithm preserves the distribution of the OFDM signal except for a slight change in the tail of the distribution. Indeed, when the power control P_{PC} increases, the tail of the TR-QCQP PDF decreases and the contribution of the minor modes increases. Therefore, the $D_{\text{QCQP}}^*(R)$ of a tone-reserved signal is farther from the Gaussian upper bound.

In summary, to infer the gain obtained when the distribution of the signal to be compressed is non-Gaussian, the relative distortion reduction of the clipped and tone-reserved PAPR-reduced IQ samples PDFs relative to the Gaussian PDF, i.e., $D_G^*(R) - D_{\text{clip}}^*(R)$ and $D_G^*(R) - D_{\text{QCQP}}^*(R)$, respectively, are summarized in column 2 of Table I.

Moreover, for the sake of clarification and comparison, Fig. 8 shows the asymptotic scalar quantization distortion defined in Proposition 1, i.e., *Panter and Dite formula* for Gaussian, for clipped and tone-reserved signals together with their SLB. The asymptotic scalar quantization distortion is calculated from the following closed-form expression for the Gaussian signal, $D_{\text{LQ}}^G = \frac{\pi\sqrt{3}}{2}\sigma^2 2^{-2R}$ [28], derived in (44) for the clipped signal and computed numerically for the tone-reserved signal. The difference between the asymptotic

TABLE I
DISTORTION REDUCTION FOR CLIPPED AND TR-QCQP SIGNALS,
RELATIVE TO THE GAUSSIAN-DISTRIBUTED SIGNAL AND THE
ASYMPTOTIC DIFFERENCE IN DISTORTION BETWEEN THE LLOYD
QUANTIZER AND SLB FOR EACH PDF

PDF	$D_G^*(R) - D^*(R)$	$D_{LQ}(R) - D^*(R)$
Gaussian PDF	0	4.34 dB
TR-QCQP, $P_{PC} = 10$ dB	0.83 dB	2.52 dB
TR-QCQP, no power limit	1.24 dB	2.26 dB
Clipped, ($\Lambda = 1.59$ dB)	2.0 dB	2.97 dB
Clipped, ($\Lambda = 1.07$ dB)	2.72 dB	3.47 dB
Clipped, ($\Lambda = 0.51$ dB)	3.72 dB	3.60 dB

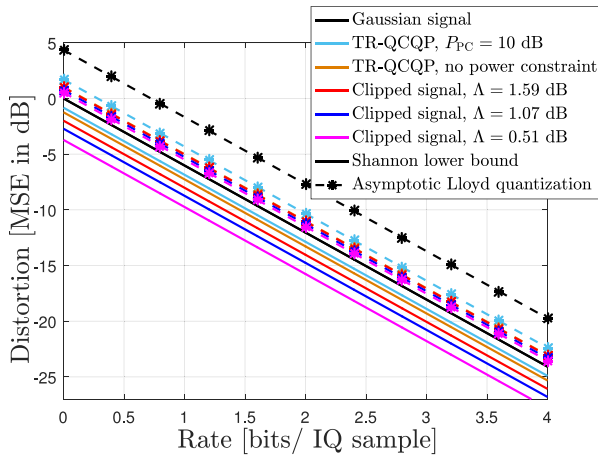


Fig. 8. Asymptotic distortion of Lloyd quantizer and SLB for clipped and TR-QCQP PAPR-reduced signals, at different Λ and P_{PC} , respectively, vs resolution.

quantization distortion and SLB for each PDF is summarized in column 3 of Table I. Obviously, the Lloyd quantizer can achieve lower MSE, i.e., better performance by approaching SLB for clipped and tone-reserved signals than for the Gaussian signal.

C. Gaussian Quantizer Performance Evaluation

In this section, the robustness of Gaussian-optimized compression techniques when applied to a PAPR-reduced signal is evaluated. The results are given thanks to the SQNR to highlight the effect of the quantization block.

1) *Clipping*: Fig. 9 shows the simulated SQNR w.r.t. the clipping ratio Λ for different resolutions. The solid lines represent the optimal performance of the Gaussian quantizer applied to a Gaussian OFDM signal. The dashed lines represent the SQNR obtained when the Gaussian quantizer is applied to the clipped IQ samples. We first conclude that applying a Gaussian quantizer to a clipped signal results in a severe degradation of the SQNR. Moreover, the performance loss increases as the resolution of the quantizer increases. Finally, the higher the clipping threshold Λ , the lower the performance loss, since the distribution of clipped IQ samples converges to a zero-mean Gaussian distribution. Therefore, the SQNR curves reach a constant ceiling at high clipping thresholds.

2) *TR With QCQP Solution*: Fig. 10 shows the simulated MER as a function of the resolution R for different values of P_{PC} and N_{PRT} , respectively. The solid line represents the

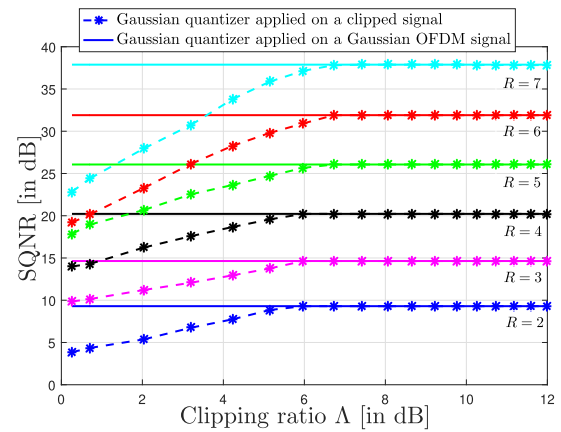


Fig. 9. SQNR vs clipping ratio Λ of a Gaussian quantizer applied on a clipped signal vs the resolution.

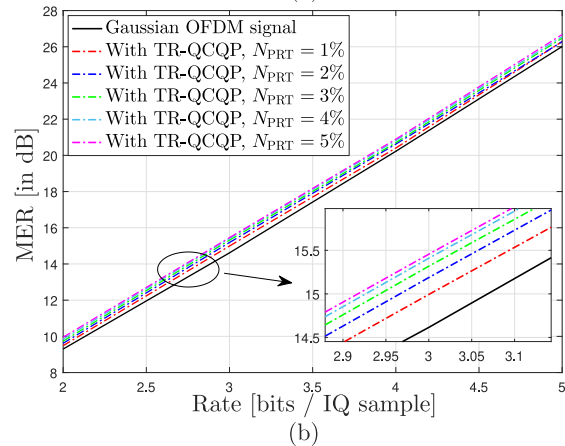
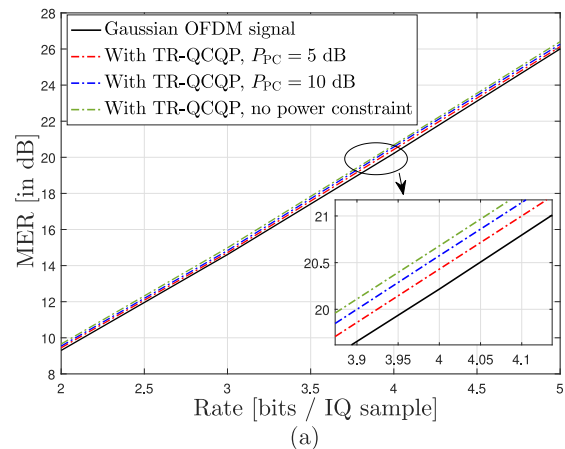


Fig. 10. MER vs resolution of a Gaussian quantizer applied to a TR-QCQP signal. (a) different power constraints P_{PC} and $N_{PRT} = 1\%$. (b) different percentages of PRTs N_{PRT} and $P_{PC} = 10$ dB.

optimal performance of a Gaussian quantizer applied to a Gaussian OFDM signal. The dashed lines represent the MER obtained when the Gaussian quantizer is applied to the tone-reserved PAPR-reduced IQ samples. We first note that using a Gaussian quantizer on a tone-reserved signal does not lead to any performance degradation, on the contrary, a slight improvement in the MER performance is obtained compared to the Gaussian case. Moreover, MER is getting better when

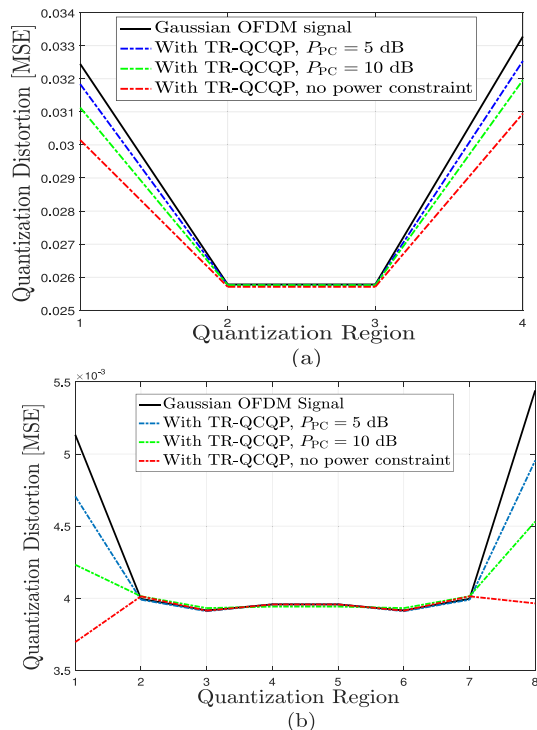


Fig. 11. MSE per each quantization region for different power constraints. (a) 4-level quantizer with 2 bits per sample. (b) 8-level quantizer with 3 bits per sample.

increasing P_{PC} or N_{PRT} . This can be explained as follows based on our previous analysis. The main mode follows the Gaussian distribution. Therefore, the Gaussian codebook quantization levels in this region is optimally adapted. On the other hand, the tail of the distribution is reduced when increasing P_{PC} or N_{PRT} which means that high amplitude values occur with quasi-null probability, resulting in lower quantization distortion compared to purely Gaussian distributed samples. We show the partial quantization distortion experienced by each quantization region for 4 and 8 level quantizers in Fig. 11a) and Fig. 11b), respectively. The quantization distortion of tone-reserved signals is reduced on the first and last regions, compared to the distortion on the OFDM signal, while they are the same in other regions, since the distributions are quite similar.

D. Comparison of Gaussian and Optimized Quantizers

Even though the Gaussian quantizer has been shown to be very robust to the modification in the distribution of the samples after PAPR reduction in some situations, this does not mean that no gain can be expected from an optimized quantizer. In this section, we therefore use the obtained distribution of the PAPR-reduced IQ samples to study the gain in system performance obtained by optimizing the compression techniques.

1) *Clipping*: In Fig. 12, the analytical expression of the MER provided in Lemma 3 is validated by plotting the analytical and simulated MER as a function of the clipping ratio Λ for different resolutions. Due to the precision of the asymptotic quantization distortion formula in Proposition 1, the analytical

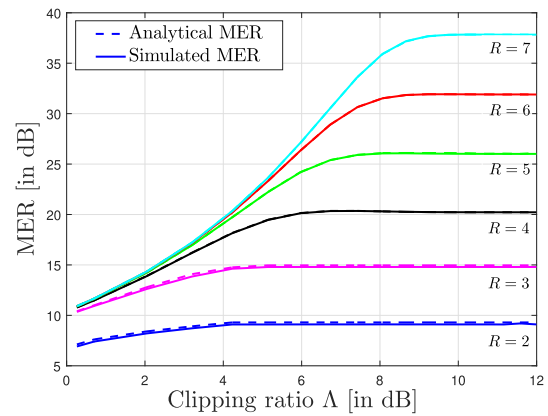


Fig. 12. Simulated and analytical MER vs clipping ratio Λ of clipped optimized compression techniques for different resolutions.

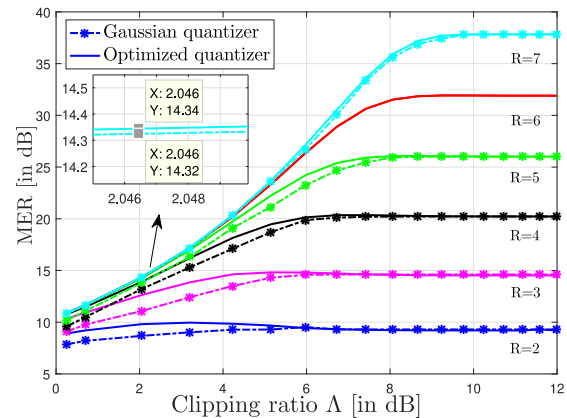


Fig. 13. MER of Gaussian and optimized compression techniques vs clipping ratio Λ for different resolutions.

expression of MER at high resolutions agrees perfectly with the simulation results, as long as $R \geq 4$ [28]. Moreover, the difference between the theoretical and simulated MER does not exceed 0.25 dB at low resolution, which validates the proposed MER expression.

Fig. 13 shows the MER for both Gaussian and clipped optimized compression techniques obtained from the proposed analytical study as a function of the clipping ratio Λ for different resolutions. First, MER increases as the clipping ratio increases and at high clipping ratios, only the quantization distortion affects the system performance. Second, the higher the clipping ratio, the more the signal distribution approaches the zero-mean Gaussian distribution. Thus, the two types of compression techniques merge to achieve an upper bound that is the MER when only the quantization distortion of a Gaussian-distributed signal at a given rate is considered. This explains the 6-dB gap between the different rates at high clipping ratios and verifies the famous 6-dB quantization rule [29].

In conclusion, applying optimized compression techniques to a clipped PAPR-reduced signal improves the performance of the MER at low resolutions and low clipping ratios, i.e., a highly clipped signal. However, compared to pure Gaussian compression schemes, the degree of improvement decreases when resolution increases, reaching about 0.02 dB when an average of 7 bits per IQ sample is used. This can

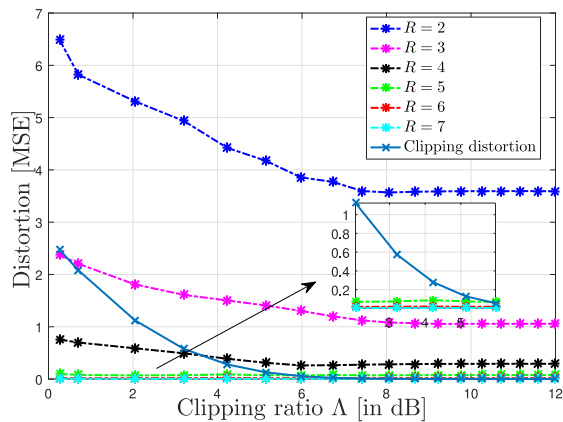


Fig. 14. Clipping PAPR-reduction and Gaussian quantizer MSEs vs clipping ratio Λ for different resolutions.

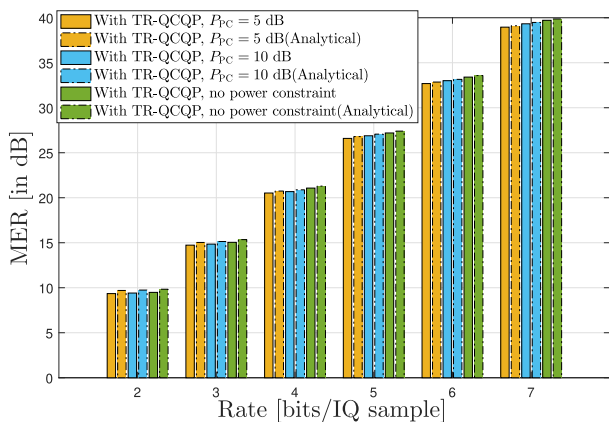


Fig. 15. Simulated and asymptotic MER vs resolution of TR-QCQP optimized compression techniques for different power constraints P_{PC} .

be explained by exploring Fig. 14, where the clipping and Gaussian quantization distortions are plotted separately for different resolutions. It can be observed that although the quantizer is not optimized for the clipped input signal, the quantization distortion is negligible compared to the clipping distortion at high rates. This is because a large number of quantization levels in a finite quantization region effectively reduces the quantization distortion to almost 0.006 even if it is not an optimized quantizer. Thus, in both cases, clipping distortion becomes the only dominant fixed distortion compared to quantization distortion.

2) *TR With QCQP Solution:* We confirm the asymptotic MER numerically, using the obtained PDF of the TR-QCQP IQ samples in Theorem 2. Fig. 15 compares the asymptotic theoretical MER with the one obtained by simulations for different power constraints on the reserved tones. Theoretical values are represented by bars bordered with dashed lines while those obtained by simulations are bars bordered by solid lines. They agree acceptably at the high rates. More precisely, the deviation between the asymptotic and simulated results is less than 0.18 dB for $R \geq 5$. This validates our theoretical findings in Theorem 2. Hence, we can use the derived IQ PDF along with the estimated parameters of the amplitude distribution in [22] to evaluate the performance of different

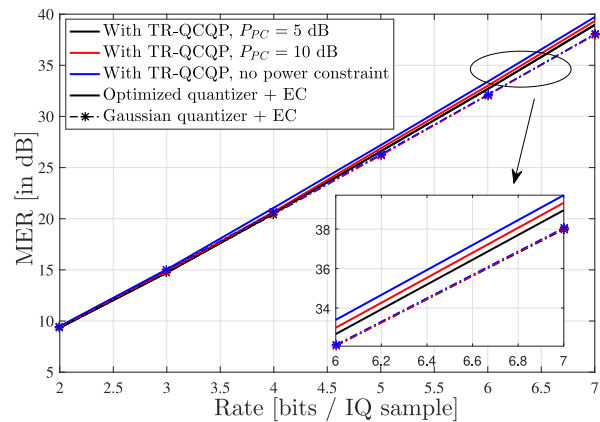


Fig. 16. MER of Gaussian and optimized compression techniques vs resolution for different power constraints P_{PC} and $N_{PRT} = 1\%$.

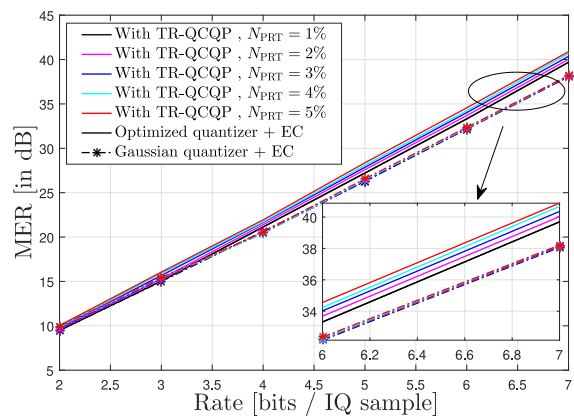


Fig. 17. MER of Gaussian and optimized compression techniques vs resolution for different percentages of PRTs N_{PRT} and $P_{PC} = 10$ dB.

compression techniques without having to perform complex and time consuming numerical simulations.

Figs. 16 and 17 show MER of both Gaussian and tone-reserved optimized compression techniques obtained by numerically integrating the IQ distribution obtained in Theorem 2 as a function of resolution R for different P_{PC} and N_{PRT} , respectively. A zoom on the high-rate region is also included. It is found that optimizing the compression techniques to the distribution of the tone-reserved signal improves the MER performance at high resolutions. Moreover, the MER performance gain increases significantly when the power constraint P_{PC} or the percentage of reserved tones for TR N_{PRT} increases.

This can be explained by the fact that higher rates, i.e., a larger number of quantization levels covering the finite quantization region, reflect the ability of the optimized codebook quantization levels to exploit the statistical changes in the tail of the distribution. Indeed, the role of the optimized compression techniques becomes more efficient when the contribution of the minor modes becomes more significant by increasing the P_{PC} or the N_{PRT} . For example for a $P_{PC} = 10$ dB and a PRT ratio of 1%, as defined in the DVB-T2 specifications, the optimized compression techniques improve the MER by about 1.6 dB compared to the purely Gaussian compression technique, when 7 bits per IQ sample are used in average.

V. CONCLUSION

This paper investigated the effect of reducing the PAPR of an OFDM signal in the time-domain before compression in a C-RAN architecture. The analytical distributions of the PAPR-reduced OFDM IQ samples have been derived and validated by simulation analysis for both clipping and QCQP PAPR reduction techniques. The obtained IQ distributions were used to optimize the codebook levels of a non-uniform scalar quantizer and the average number of bits allocated by the entropy encoder in addition to the analysis of the MER, modeling the joint effect of PAPR reduction and quantization operations.

First, by analyzing the theoretical Shannon bound for the obtained distributions of the clipped and tone-reserved signals, we show how the compression techniques take advantage of changing the distribution of the signal to be compressed. The simulation results have shown that the Gaussian-optimized quantizer is not very robust when applied to a clipped signal. Moreover, the gain of using an optimized quantizer considering the clipping operation is highlighted, especially in the low-rate quantization region. However, the gain decreases significantly in the high-rate region. While, in the case of the TR-QCQP algorithm, the Gaussian quantizer works properly when applied to a tone-reserved signal, because the distribution of the latter is close to a Gaussian one. However, we show that the optimized quantizer based on the distribution of the tone-reserved IQ samples fulfils a significant gain in the high-rate quantization region, especially for a high number of tones reserved for TR and high power constraint.

APPENDIX A PROOF OF THEOREM 2

The multiplication of the Rayleigh distribution by the GEV CDF in the amplitude distribution of the tone-reserved PAPR-reduced signal $f_{R_{in}}^{QCQP}(r)$ in Lemma 2 is complex to integrate. Therefore, in [22], the authors propose a suitable approximation that has been numerically tested to ensure an appropriate trade-off between the complexity of the expression and the accuracy of the computations.

The approximation consists in replacing the GEV CDF in $f_{R_{in}}^{QCQP}(r)$ in Lemma 2 by a unit step function truncated at $r_s = \mu_1 + \frac{\sigma_1}{k_1}((\ln 2)^{-k_1} - 1)$, i.e., $u(r - r_s)$. Thus, $f_{R_{in1}}(r)$ in (8) can be expressed by:

$$f_{R_{in1}}(r) = \begin{cases} q f_R^{\text{Ray}}(r)(1 - u(r - r_s)), & \text{if } r \in [0, r_s] \\ 0, & \text{otherwise,} \end{cases} \quad (50)$$

Based on this approximation and remembering that $f_{R_{in2}}(r)$ is equal to a GEV distribution over $[0, \mu_2 - \frac{\sigma_2}{k_2}]$ and 0 elsewhere. The respective support of the amplitude distribution of the TR-QCQP signal is redefined over $[0, d^*]$, where $d^* = \max(r_s, \mu_2 - \frac{\sigma_2}{k_2})$. Thus, the evaluation of $f_{X_1}(x)$ in (28) can be developed as follows:

$$f_{X_1}(x) = \int_{-d^*}^{d^*} \frac{(1-p)q}{2\pi\sigma_{\text{ray}}^2} e^{-\frac{x^2+y^2}{2\sigma_{\text{ray}}^2}} u\left(r_s - \sqrt{x^2+y^2}\right) dy. \quad (51)$$

The unit step function redefines the integral over $[-\sqrt{r_s^2 - x^2}, \sqrt{r_s^2 - x^2}]$. Then, using the integral identity

in [26, eq. (1), Sec. 3.321, p. 336], $f_{X_1}(x)$ can be expressed as in Theorem 2.

In the same way, $f_{X_2}(x)$ in (28) is evaluated from

$$f_{X_2}(x) = \frac{p}{\pi\sigma_2} \int_0^{d^*} \underbrace{\frac{1}{\sqrt{x^2+y^2}} G(x,y)^{k_2+1} e^{-G(x,y)}}_I dy. \quad (52)$$

Consider the change of variable $\psi = G(x,y)$ in I , where $G(x,y)$ is in (30). Thus,

$$\begin{aligned} \frac{d\psi}{dy} &= \frac{-y}{\sigma_2\sqrt{x^2+y^2}} \left[G(x,y)^{k_2+1} \right], \\ y &= \sqrt{\left(\mu_2 + \frac{\sigma_2}{k_2} (\psi^{-k_2} - 1) \right)^2 - x^2}, \end{aligned} \quad (53)$$

and the integral limits are stated as

$$\begin{aligned} \psi_1 &= \left[1 + \frac{k_2}{\sigma_2} (x - \mu_2) \right]^{-\frac{1}{k_2}}, \quad \text{and} \\ \psi_2 &= \left[1 + \frac{k_2}{\sigma_2} \left(\sqrt{x^2 + d^{*2}} - \mu_2 \right) \right]^{-\frac{1}{k_2}}. \end{aligned} \quad (54)$$

Hence, we get:

$$I = -\sigma_2 \int_{\psi_1}^{\psi_2} \frac{1}{\sqrt{\left(\mu_2 + \frac{\sigma_2}{k_2} (\psi^{-k_2} - 1) \right)^2 - x^2}} e^{-\psi} d\psi. \quad (55)$$

Let us assume the following notations

$$c_1 = \frac{\sigma_2^2}{k_2^2}, \quad c_2 = \frac{2\mu_2\sigma_2}{k_2} - 2c_1, \quad \text{and} \quad c_3 = \mu_2^2 - c_1 - c_2 - x^2, \quad (56)$$

and with adequately rearranging the terms, I is stated as follows

$$I = -\sigma_2 \int_{\psi_1}^{\psi_2} \underbrace{\left(c_1 \psi^{-2k_2} + c_2 \psi^{-k_2} + c_3 \right)^{-\frac{1}{2}}}_I e^{-\psi} d\psi. \quad (57)$$

Thus, using the generalized Newton multinomial theorem [30] to expand I_1 , I_1 can be developed as

$$I_1 = \sum_{p_1=0}^{\infty} \sum_{p_2=0}^{p_1} \binom{-\frac{1}{2}}{p_1} \binom{p_1}{p_2} c_1^{-\frac{(1+2p_1)}{2}} c_2^{p_1-p_2} c_3^{p_2} \psi^{k_2(p_1+p_2+1)}, \quad (58)$$

Substituting I_1 into I and using the integral property in [26, eq. (2), Sec. 8.35, p. 899]. Together with filling I into (52) and with further simplification of the expression, $f_{X_2}(x)$ can be expressed as in Theorem 2.

APPENDIX B PROOF OF LEMMA 4

For the clipping PAPR reduction case, P_s is the power of a complex Gaussian distributed signal with standard deviation σ_{ray} . Thus, $P_s = 2\sigma_{\text{ray}}^2$.

D_C and $D_{\text{LQ}}^{\text{clip}}$ are the powers of the clipping and quantization distortions, respectively, which are considered statistically

independent [31]. Let us first derive the clipping distortion D_C which can be computed as follows:

$$D_C = \mathbb{E}[|S - Z_{\text{in}}^{\text{clip}}|^2] = \mathbb{E}[(R_s - R_{\text{in}})^2], \quad (59)$$

Expanding the expectation operator and taking the clipping definition (2) into consideration leads to

$$D_C = \mathbb{E}[(R_s - R_{\text{in}})^2] = \int_{V_{\text{max}}}^{\infty} (r - V_{\text{max}})^2 f_{R_s}(r) dr. \quad (60)$$

After expanding the squared term and using the integral identity in [26, eq. (9), Sec. 3.381, p. 346], D_C can be expressed as in Lemma 3.

The asymptotic quantization distortion D_{LQ} is derived from “Panter and Dite formula” in Proposition 1. As already shown in Section III-A, the in-phase and the Quadrature-phase of a PAPR-reduced complex signal are identical at the input of the quantizer. Therefore, the quantization distortion is the same for both components and can be derived for complex samples as follows:

$$D_{\text{LQ}}^{\text{clip}} = \frac{2^{-2R}}{6} \left(\underbrace{\int_{-\infty}^{\infty} \sqrt[3]{f_X^{\text{clip}}(x)} dx}_I \right)^3. \quad (61)$$

The evaluation of (61) using the PDF of the clipped IQ samples given in Theorem 1 leads to the following integral derivation,

$$I = \int_{-V_{\text{max}}}^{V_{\text{max}}} \left(\frac{1}{\sqrt{2\pi\sigma_{\text{ray}}^2}} e^{-\frac{x^2}{2\sigma_{\text{ray}}^2}} \operatorname{erf}\left(\frac{V_{\text{max}}}{\sqrt{2\sigma_{\text{ray}}^2}}\right) + \frac{e^{-\Lambda}}{2\pi} \frac{1}{\sqrt{V_{\text{max}}^2 - x^2}} \right)^{\frac{1}{3}} dx. \quad (62)$$

Let us assume the following notations

$$a = \frac{1}{\sqrt{2\pi\sigma_{\text{ray}}^2}} \operatorname{erf}\left(\frac{V_{\text{max}}}{\sqrt{2\sigma_{\text{ray}}^2}}\right), \quad b = \frac{1}{2\sigma_{\text{ray}}^2}, \quad \text{and} \quad c = \frac{e^{-\Lambda}}{2\pi}. \quad (63)$$

Thus, using the generalized Newton binomial theorem [30], I can be developed as

$$\begin{aligned} I &= \int_{-V_{\text{max}}}^{V_{\text{max}}} \sum_{k=0}^{\infty} \binom{\frac{1}{3}}{k} (ae^{-bx^2})^{\frac{1}{3}-k} \left(\frac{c}{\sqrt{V_{\text{max}}^2 - x^2}} \right)^k dx \\ &= \sum_{k=0}^{\infty} \binom{\frac{1}{3}}{k} \int_{-V_{\text{max}}}^{V_{\text{max}}} \frac{(ae^{-bx^2})^{\frac{1}{3}-k} c^k}{(\sqrt{V_{\text{max}}^2 - x^2})^k} dx, \end{aligned} \quad (64)$$

Rearranging the terms in I leads to

$$I = \sum_{k=0}^{\infty} \binom{\frac{1}{3}}{k} c^k a^{\frac{1-3k}{3}} \underbrace{\int_{-V_{\text{max}}}^{V_{\text{max}}} \frac{e^{-\frac{b(1-3k)x^2}{3}}}{(\sqrt{V_{\text{max}}^2 - x^2})^k} dx}_{I_1}. \quad (65)$$

Thus, with proper variable substitution along with the integral property in [26, eq. (1), Sec. 3.383, p. 347], I_1 is solved as

$$I_1 = \frac{1}{b^{\frac{1-k}{2}}} \left[B\left(\frac{2-k}{2}, \frac{1}{2}\right) (dV_{\text{max}}^2)^{\frac{1-k}{2}} \times {}_1F_1\left(\frac{1}{2}; \frac{3-k}{2}; -dV_{\text{max}}^2\right) \right] \text{ with } k \leq 1, \quad (66)$$

where $d = \frac{b(1-3k)}{6\sigma^2}$. Finally, substituting I_1 into I , filling I into (61), and with further simplifications of the expression, $D_{\text{LQ}}^{\text{clip}}$ can finally be expressed as in Lemma 3.

Finally, $P_{z_{\text{in}}}^{\text{clip}}$ is the power of a complex clipped IQ sample, computed with the distribution in Theorem 1, i.e.,

$$P_{z_{\text{in}}}^{\text{clip}} = 2 \int_{-V_{\text{max}}}^{V_{\text{max}}} x^2 f_X^{\text{clip}}(x) dx. \quad (67)$$

Using the integral identity in [26, eq. (5), Sec. 3.321, p. 336] for the exponential function, $P_{z_{\text{in}}}^{\text{clip}}$ is expressed as shown in Lemma 3.

REFERENCES

- [1] A. Checko *et al.*, “Cloud RAN for mobile networks—A technology overview,” *IEEE Commun. Surveys Tuts.*, vol. 17, no. 1, pp. 405–426, 1st Quart., 2014.
- [2] A. Pizzinat, P. Chanclou, F. Saliou, and T. Diallo, “Things you should know about fronthaul,” *J. Lightw. Technol.*, vol. 33, no. 5, pp. 1077–1083, Mar. 1, 2015.
- [3] I. Chih-Lin, J. Huang, R. Duan, C. Cui, J. Jiang, and L. Li, “Recent progress on C-RAN centralization and cloudification,” *IEEE Access*, vol. 2, pp. 1030–1039, 2014.
- [4] “5G; procedures for the 5G system, version 15.2.0 release 15,” Eur. Telecommun. Stand. Inst., Sophia Antipolis, France, Rep. 3GPP TS 23.502, Mar. 2019.
- [5] *Frame Structure Channel Coding and Modulation for a Second Generation Digital Terrestrial Television Broadcasting System (DVB-T2), V1.1.1*, ETSI Standard EN 302755, Sep. 2009.
- [6] *ATSC Proposed Standard: Physical Layer Protocol*, document S32-230r56, Adv. Telev. Syst. Committee, Washington, DC, USA, 2016.
- [7] J. Lee, E. Hyun, and J.-Y. Jung, “A simple and efficient IQ data compression method based on latency, EVM, and compression ratio analysis,” *IEEE Access*, vol. 7, pp. 117436–117447, 2019.
- [8] A. Shehata, M. Crussière, and P. Mary, “Analysis of baseband IQ data compression methods for centralized RAN,” in *Proc. IEEE 28th Eur. Signal Process. Conf. (EUSIPCO)*, 2021, pp. 1762–1766.
- [9] A. Vosoughi, M. Wu, and J. R. Cavallaro, “Baseband signal compression in wireless base stations,” in *Proc. IEEE Global Commun. Conf. (GLOBECOM)*, 2012, pp. 4505–4511.
- [10] B. Guo, W. Cao, A. Tao, and D. Samardzija, “LTE/LTE-a signal compression on the CPRI interface,” *Bell Labs Tech. J.*, vol. 18, no. 2, pp. 117–133, 2013.
- [11] H. Si, B. L. Ng, M. S. Rahman, and J. Zhang, “A novel and efficient vector quantization based CPRI compression algorithm,” *IEEE Trans. Veh. Technol.*, vol. 66, no. 8, pp. 7061–7071, Aug. 2017.
- [12] Y. Su, M. LiWang, L. Huang, X. Du, and N. Guizani, “Green communications for future vehicular networks: Data compression approaches, opportunities, and challenges,” *IEEE Netw.*, vol. 34, no. 6, pp. 184–190, Nov./Dec. 2020.
- [13] L. Ramalho, I. Freire, C. Lu, M. Berg, and A. Klautau, “Improved LPC-based fronthaul compression with high rate adaptation resolution,” *IEEE Commun. Lett.*, vol. 22, no. 3, pp. 458–461, Mar. 2018.
- [14] F. Brito, M. Berg, C. Lu, L. Ramalho, I. Sousa, and A. Klautau, “A Fronthaul signal compression method based on trellis coded quantization,” in *Proc. IEEE Latin-Amer. Conf. Commun. (LATINCOM)*, 2019, pp. 1–6.
- [15] Y. Su, X. Lu, L. Huang, X. Du, and M. Guizani, “A novel DCT-based compression scheme for 5G vehicular networks,” *IEEE Trans. Veh. Technol.*, vol. 68, no. 11, pp. 10872–10881, Nov. 2019.
- [16] T. Jiang and Y. Wu, “An overview: Peak-to-average power ratio reduction techniques for OFDM signals,” *IEEE Trans. Broadcast.*, vol. 54, no. 2, pp. 257–268, Jun. 2008.

- [17] Y.-C. Wang and Z.-Q. Luo, "Optimized iterative clipping and filtering for PAPR reduction of OFDM signals," *IEEE Trans. Commun.*, vol. 59, no. 1, pp. 33–37, Jan. 2011.
- [18] J. Tellado and J. M. Cioffi, "Peak power reduction for multicarrier transmission," in *Proc. IEEE GLOBECOM*, vol. 99, 1998, pp. 5–9.
- [19] Y. Rahmatallah and S. Mohan, "Peak-to-average power ratio reduction in OFDM systems: A survey and taxonomy," *IEEE Commun. Surveys Tuts.*, vol. 15, no. 4, pp. 1567–1592, 1st Quart., 2013.
- [20] A. Shehata, P. Mary, and M. Crussière, "Compression of clipped OFDM IQ samples for cloud radio access network," in *Proc. IEEE 32nd Annu. Int. Symp. Pers. Indoor Mobile Radio Commun. (PIMRC)*, 2021, pp. 777–782.
- [21] A. Cheaito, M. Crussière, J.-F. Héland, and Y. Louët, "Quantifying the memory effects of power amplifiers: EVM closed-form derivations of multicarrier signals," *IEEE Wireless Commun. Lett.*, vol. 6, no. 1, pp. 34–37, Feb. 2017.
- [22] M. El Hassan, M. Crussière, J.-F. Héland, Y. Nasser, and O. Bazzi, "EVM closed-form expression for OFDM signals with tone reservation-based PAPR reduction," *IEEE Trans. Wireless Commun.*, vol. 19, no. 4, pp. 2352–2366, Apr. 2020.
- [23] S. Lloyd, "Least squares quantization in PCM," *IEEE Trans. Inf. Theory*, vol. IT-28, no. 2, pp. 129–137, Mar. 1982.
- [24] D. A. Huffman, "A method for the construction of minimum-redundancy codes," *Proc. IRE*, vol. 40, no. 9, pp. 1098–1101, 1952.
- [25] P. Panter and W. Dite, "Quantization distortion in pulse-count modulation with nonuniform spacing of levels," *Proc. IRE*, vol. 39, no. 1, pp. 44–48, 1951.
- [26] A. Jeffrey and D. Zwillinger, *Table of Integrals, Series, and Products*. Amsterdam, The Netherlands: Elsevier, 2007.
- [27] M. C. Thomas and A. T. Joy, *Elements of Information Theory*, vol. 3. New York, NY, USA: Wiley, 1991, pp. 37–38.
- [28] J. Makhoul, S. Roucos, and H. Gish, "Vector quantization in speech coding," *Proc. IEEE*, vol. 73, no. 11, pp. 1551–1588, Nov. 1985.
- [29] A. Gersho and R. M. Gray, *Vector Quantization and Signal Compression*, vol. 159. New York, NY, USA: Springer, 2012.
- [30] C.-S. Liu, "The essence of the generalized Newton binomial theorem," *Commun. Nonlinear Sci. Numer. Simulat.*, vol. 15, no. 10, pp. 2766–2768, 2010.
- [31] M. Bernhard, D. Rörich, T. Handte, and J. Speidel, "Analytical and numerical studies of quantization effects in coherent optical OFDM transmission with 100 Gbit/s and beyond," in *Proc. ITG Fachtagung Photonische Netze*, 2012, pp. 34–40.



Aya Shehata received the B.Sc. and M.Sc. degrees in communication engineering from the German University, Cairo, in 2014 and 2016. She is currently pursuing the Ph.D. degree in communication and electronics with the Institute for Electronics and Telecommunications, National Institute of Applied Sciences, Rennes, France. Her research interests include digital signal processing, source coding, and multicarrier communication systems.



Philippe Mary (Member, IEEE) received the Graduation degree in signal processing and digital communications from the University of Côte d'Azur in 2004, France, the Ph.D. degree in electrical engineering from the Institut National des Sciences Appliquées de Lyon in 2008, France, and the Habilitation à Diriger les Recherches from the University of Rennes in 2018, France.

He has been an Associate Professor with INSA Rennes and a Member of IETR Laboratory since 2009, France. During the Ph.D. degree, he was with France Telecom R&D, Grenoble, France, and he worked on the analytical performance study for mobile communications considering shadowing and fading and multi-user detectors for wireless communications. In 2008, he held a post-doctoral position with ETIS Laboratory, Cergy-Pontoise, France, during 12 months and he was a Teaching Assistant with ENSEA and University of Cergy-Pontoise. Since 2009, he has been leading and contributing to several industrial and academic projects, and developed several collaborations with various Universities. He also served in several international conference technical program committees and he organized two international workshops and one winter school on signal processing and information theory for IoT. His research interests include signal processing for wireless communications and information and communication theory.



Matthieu Crussière received the M.Sc. and Ph.D. degrees in electrical engineering from the National Institute of Applied Sciences, Rennes, France, in 2002 and 2005, respectively.

In 2007, he joined the Department of Telecommunications and Electronic Engineering with INSA as an Associate Professor. From 2016 to 2021, he was the Head of the Signal and Communication Research Team of the Electronics and Telecommunications Institute of Rennes. In 2014, he started collaborations as an Associate Researcher with the Institute of Research and Technology B-COM, Rennes. Since 2021, he has been with the Head of the Electronics and Telecommunications Engineering Department, INSA as a Full Professor and holds a transverse research program with IETR about the evolution of future communication systems towards mmWaves and sub-THz bands. His first works were focused on the optimization of high-bit rate powerline communications using hybrid multicarrier and spread-spectrum waveforms. Then he developed an expertise in adaptive resource allocation, optimization algorithms and system design for multicarrier and multiantenna systems. This last years, he has developed various research axes around the optimization of the physical layer of next generation mobile systems and networks (beyond 5G), mixing traditional signal processing approaches and deep learning tools. He has authored or coauthored of more than 150 technical papers in international conferences and journals and holds more than 10 patents. He has been involved in several European and French National Research Projects in the field of powerline communications, broadcasting systems, ultra wideband, and mobile radio communications. His main research interests lie in digital communications and signal processing techniques applied to communication systems.